Graphene Supported Monometallic and Bimetallic Dimers for Electrochemical CO_2 Reduction

Haiying He,[1*] Christopher Morrissey,[1] Larry A. Curtiss[2] and Peter Zapol[2*]

[1]*Department of Physics and Astronomy, Valparaiso University, Valparaiso, IN 46383*

[2]*Materials Science Division, Argonne National Laboratory, Lemont, IL 60439*

August 13, 2018

Abstract

Bimetallic catalysts are attractive alternatives to extend the parameter space that can be tuned for support interactions and catalytic performance. In this study, we have investigated the smallest bimetallic catalysts - dimers - supported on defective graphene for the electrochemical reduction of CO_2 to CH_4 based on a first-principles approach and the computational hydrogen electrode model. The monometallic and bimetallic dimers formed from Group 10 (Ni, Pd, Pt) and group 11 (Cu, Ag, Au) elements are characterized by a positively charged anchoring atom occupying the vacancy site of graphene and a neutral or slightly negatively charged antenna atom sticking out from the graphene surface. The strong selective binding of these dimers ensures their high stability. Possible rate limiting steps are identified from the full reaction pathways to generate CH_4. Overall, Pt_2, AgNi, Pd_2, and AgPt are the best candidates with the lowest overpotential values of 0.37, 0.69, 0.69 and 0.76 V, respectively. It is found that the alloy effect and the interaction with support help to optimize the property. These metallic dimers, however, retain nonmonotonous property relationships that give opportunity to go beyond scaling behavior and look for a few atom catalysts that have unique properties to reduce rate limiting potentials and improve the catalytic performance.

* corresponding authors: haiying.he@valpo.edu; zapol@anl.gov

I. INTRODUCTION

Conversion of CO_2 into useful chemicals or fuels using electrical energy is a topic of great interest to both fundamental electrochemistry and potential industrial applications. The electrochemical method[1-4] offers direct utilization of renewable electricity (e.g., production of solar fuels), and holds promise for both high selectivity and efficiency. As the key part in electrochemical reduction of CO_2, the electrodes fulfill dual roles as both electron conducting medium and catalytically active sites. The development of electrodes has gone from single-crystal metal electrodes,[5] to supported metal nanoparticle electrodes.[6-9] Superior catalytic performance has been found for supported size-selected subnanometer metal clusters (composed of a few atoms)[10-12] which can be attributed to the unique electronic structure as the size of the cluster is reduced, the high specific surface area, and the significant effect of the underlying support beyond the active sites. In addition, the use of very small clusters can largely reduce the amount of catalytically active materials needed, especially for precious metals such as Au, Pt, and Pd.

In a recent work, we have studied the single metal atoms supported on defective graphene sheets as electrocatalysts for CO_2 conversion using the first-principles approach.[13] These single atoms behave quite differently from their bulk counterparts due to the distinctly different electronic structure. Reduction in the overpotentials for producing methane and methanol were observed. Activity improvements were also reported recently by Jung's group.[14] It opens a new horizon in the development of electrocatalysts for CO_2 reduction.

Metal alloys provide a large parameter space to tune electronic structure that can be investigated theoretically[15, 16] and were shown experimentally to deliver superior electrocatalytic activity.[17, 18] At the same time, correlations between electrochemical performance and alloy

composition of the electrocatalyst surface impose limitations on reducing overpotentials, expressed as "volcano" plots.[16] There are very few theoretical or experimental studies that have explored electrochemical activity of supported bimetallic clusters.[19, 20] Particularly, we address the following questions. Do the unique electronic structures of clusters lead to different property correlations that can enable overcoming of performance limitations for CO_2 reduction? What fundamental physical or chemical properties correlate with activity and selectivity of these subnanometer clusters? How does performance depend on composition of the supported clusters?

In this work, we start with evaluation of the stability of monometallic and bimetallic dimers on defective graphene followed by assessment of their favorability of CO_2 reduction reaction (CRR) over hydrogen evolution reaction (HER). The full reaction pathways for CO_2 reduction were then investigated on graphene-supported monometallic dimers M_2 (M= group 10: Ni, Pd, Pt; and group 11: Cu, Ag, Au). This choice of metals is based on our results indicating that these metals are the best candidates for CO_2 reduction using graphene supported single atom catalysts.[13] It was found that the OH binding energy to single metal atoms shows a good correlation with the elemental group number of the metal in the periodic table and decreases with the increase in the group number. Group 10 and 11 elements demonstrate the best catalytic performance for CH_4 production. By analyzing these typical pathways, we identify rate limiting steps with a special focus on the $8e^-$ reduction to generate the highest energy compound methane (CH_4). Although CH_4 is not an ideal product for utilization, the fundamental study of reaction pathways and rate limiting steps for this reaction may serve as the first step in understanding pathways leading to the more desirable longer-chain hydrocarbons.

Lastly, we do a computational screening of bimetallic dimers MN (M= group 11: Cu, Ag, Au; and N= group 10: Ni, Pd, Pt) to find the lowest overpotential for CO_2 reduction to methane. The

bimetallic dimer is formed by one element from group 10 and one from group 11. Therefore, a total of 9 different compositions are considered. The reaction overpotentials are then correlated with the composition of the alloy clusters. This will help to understand how to design new classes of electrocatalysts to overcome performance bottlenecks inherent to extended surface catalysts.

II. COMPUTATIONAL MODEL AND METHODS

All the calculations were done within the framework of the density functional theory (DFT) with periodic boundary conditions as implemented in the VASP program.[21] The PBE exchange-correlation functional[22] and the van der Waals (vdW) interactions described via a pair-wise force field using the DFT-D2 method of Grimme[23] were chosen for all calculations. The projector augmented wave (PAW) method and plane wave basis set were used with energy cutoff of 400 eV. All of the atoms are allowed to relax during the structure optimization. The total energy was converged to 10^{-5} eV, and the geometry was relaxed until the force on each atom was below 0.03 eV/Å. Bader charge analysis[24] was done to analyze charge populations.

Six monometallic metal dimers M_2 (M= Cu, Ag, Au, Ni, Pd, Pt,) and nine bimetallic dimers MN (M= Cu, Ag, Au; N= Ni, Pd, Pt,) were selected for the detailed investigation of reaction pathways to produce CH_4. Graphene with single C vacancies was chosen as the support, where these metal dimers were anchored at the vacancy sites.[25] The defective graphene was modeled using a 5 ×5 supercell. A vacuum layer with a minimum thickness of 15 Å was placed along the *z* direction in the presence of all possible adsorbates. The size of the supercell was chosen to be large enough to reasonably neglect the interaction between imaging cells, and small enough to be computationally effective.

We used the computational hydrogen electrode (CHE) model,[16, 26, 27] and applied zero point energy, entropy and solvation energy corrections to obtain the thermodynamics of elementary reaction steps. Details of the thermodynamic corrections were described by Nørskov's group.[27] Considering the similarity in the metallic supports (graphene) for different dimer systems, we have considered the water solvation implicitly by including the solvation energy corrections primarily based on the functional groups of surface species. A more rigorous approach is to include explicit water molecules in the simulation as done in a recent study.[28]

III. **RESULTS AND DISCUSSION**

1. Stability of Monometallic and Bimetallic Dimers on Single-Vacancy Graphene

It is crucial to have the metallic clusters well dispersed and immobilized on the support to avoid the agglomeration of clusters and their deactivation in catalytic reactions. We have introduced single vacancies in graphene as the anchoring sites for metallic dimers. The removal of a carbon atom from graphene leaves three C atoms around the vacancy undercoordinated, which is highly attractive to metal atoms. We have first investigated the stability of the monometallic and bimetallic dimers by searching for their lowest-energy binding configurations. The M_2 and MN dimers were taken at different orientations with respect to the defective graphene and the systems were fully relaxed. In addition, in the bimetallic cases, different starting configurations with either M or N atoms at the vacancy sites were tested to compare the energetic stability of the optimized structures. The binding energy of anchoring an alloy dimer MN (equally applicable to a M_2 dimer) at the single vacancy site of graphene (V_C) is defined as

$$E_b[MN] = E_{V_C} + E_{MN} - E_{MN_C} \quad (1)$$

where E_{MN_C}, E_{V_C}, and E_{MN} stand for the total energy of the graphene supported MN dimer, the graphene with a single vacancy, and the isolated clusters, respectively. This binding energy measures how strongly the dimers are bound to the surface, and high binding energy prevents their diffusion/agglomeration. The more positive the value of E_b [MN], the more kinetically stable the supported cluster.

The energetics and charge distributions of the most stable configurations are listed in Table 1. The optimized structures of the lowest energy configurations can be found in Figure S1 (Supporting Information). All the binding energies are positive ranging from 2.03 eV (Ag_2) to 7.90

Table 1. Energetics and structural properties of metal dimers supported on defective graphene. Binding energy E_b [MN] (eV), charges on metal atoms Q [M] (e), Q [N] (e), and M-N bond length R [M-N] (Å) are listed on the first, second and third line of each box (for composition MN), respectively.

M_2/MN	Ni_2	Pd_2	Pt_2
E_b [MN] (eV)	7.23	6.98	7.90
Q [M] (e), Q [N] (e)	0.08, 0.45	-0.02, 0.30	-0.20, 0.34
R [M-N] (Å)	2.25	2.60	2.53
Cu_2	CuNi	CuPd	CuPt
3.82	6.17	5.17	6.63
0.19, 0.47	0.12, 0.45	-0.16, 0.28	-0.09, 0.20
2.32	2.21	2.31	2.28
Ag_2	AgNi	AgPd	AgPt
2.03	6.04	5.21	6.65
-0.18, 0.33	-0.14, 0.49	-0.17, 0.31	-0.15, 0.25
2.60	2.40	2.57	2.54

Au_2	AuNi	AuPd	AuPt
3.61	6.46	5.70	7.37
-0.30, 0.32	-0.42, 0.57	-0.40, 0.40	-0.33, 0.42
2.52	2.34	2.48	2.46

eV (Pt_2), ensuring the immobilization of these clusters on defective graphene support. Among the monometallic dimers, Group 10 dimers show stronger binding strength than Group 11 dimers at the single vacancy sites owing to the larger number of unpaired d electrons. A strong-weak-strong subgroup (Ni-Pd-Pt, Cu-Ag-Au) variation in interaction is also seen similar to the case of single atoms.[13] The Group 11 dimer Ag_2 is the least stable, the same as we have observed for the single atom binding at the single vacancy site of graphene.[13] It is no surprise that all bimetallic dimers tend to bind to the support through the Group 10 elements (Ni, Pd, Pt).[13, 29] Therefore, the stability for the alloy dimers is largely determined by the binding strength of the anchoring atoms, the Group 10 elements, which is highly enhanced compared to the monometallic cases of Cu_2, Ag_2, and Au_2. In order to further evaluate the kinetic stability, we have calculated the activation barrier for the AgNi dimer to move from the most stable binding site (E_b = 6.04 eV) to the nearest meta-stable site (E_b = 1.22 eV, a hole site as labeled in Figure S2). The calculated barrier is 4.99 eV, which is so high that it will prevent any significant sintering even under operating potentials.

One of the metal atoms of the dimer ("anchoring atom") forms three bonds nearly symmetrically with the C atoms near the vacancy site. This leads to a relatively large electron depletion for the anchoring atom. The other atom M of the dimer ("antenna atom") either forms one M-C bond with a surface C atom as in Cu_2, Ni_2, Pd_2 or Pt_2; or sticks out nearly perpendicularly as in the rest of the dimers (see Figure S1 in the Supporting Information). All the antenna atoms are negatively charged except the cases of Ni_2, Cu_2 and CuNi (Table 1), which is likely due to the

much lower electronegativity of Ni (1.91) and Cu (1.90).[30, 31] Moreover, for bimetallic dimers, the difference in charges on N and M (ΔQ [N–M]) is found linearly correlated with the difference in their electronegativity (See Supporting Information Figure S3). The total electron transfer from a metal dimer towards graphene is related to the weighted electronegativity of the metal dimer $\chi_{MN} = 0.69\chi_N + 0.31\chi_M$ based on a linear fitting of the calculated sum of charges on the metal clusters MN and the electronegativity of constituent elements χ_M and χ_N on the Pauling scale.[30, 31] (See Supporting Information Figure S4). Here we have evaluated the effective electronegativity χ_{MN} of the dimer MN using linear weighted contributions of the constituent elements. The fitted result suggests that both atoms of the dimer have an influence on the amount of charge transferred between the cluster and the support. Secondly, the effect from the anchoring atom at the vacancy site has a larger weight (~70%) indicating a larger impact on charge transfer. This charge transfer has a significant impact on the reactivity of the dimers. This effect will be further illuminated in Section III-4 when we discuss the binding strength of the supported dimers highlighting the difference among the anchoring and antenna atoms. The M-N bond lengths (R [M-N]) of supported MN dimers are listed in Table 1. For the bimetallic dimers, the M-N bond length is shorter than the algebraic average of the M-M and N-N bond lengths. This is likely due to the enhanced charge transfer because of the difference in the electronegativity of two different elements in a heteronuclear bond.

2. Favorability of CRR over HER

The H_2 evolution reaction (HER) is often a competing reaction with the CO_2 reduction reaction (CRR). As a first step in CRR, the first transfer of electron and proton, could generate typically

two possible adsorbed intermediates: COOH* and OCHO*, in competition with the first step in HER, the adsorption of H (H*), as illustrated below.

$$* + CO_2 + H^+ + e^- \rightarrow COOH* \quad (2)$$

$$* + CO_2 + H^+ + e^- \rightarrow OCHO* \quad (3)$$

$$* + H^+ + e^- \rightarrow H* \quad (4)$$

The reaction free energies of producing COOH* and OCHO* are plotted against the free energy of adsorbing H* on graphene supported metal dimers in Figure 1. Binding configurations are shown in Supporting Information Figure S5 and S6. The protonation of C to form the formate group (OCHO*) is energetically more favorable than the protonation of O to form the carboxyl group (COOH*) for all monometallic and bimetallic cases. This is very similar to what was found for single-vacancy graphene supported single metal atoms[13] and indicates that the dimers maintain the single atom properties more than the collective behaviors of clusters or particles[12,3] in terms of binding. In all cases except for Au_2, OCHO* forms a bidentate binding configuration through both oxygens to both atoms of the dimer; while in case of COOH*, the binding is primarily through the C atom, which has an unpaired sp^3 electron, to one of the metal atoms. For $COOH^*$, the C atom shows a stronger affinity to the antenna atom with exception for AgNi, AgPt and AuPt. An additional bond is formed between the oxygen in the carbonyl group C=O and the second metal atom of the dimer in the monometallic dimers, and CuNi and CuPd bimetallic dimers.

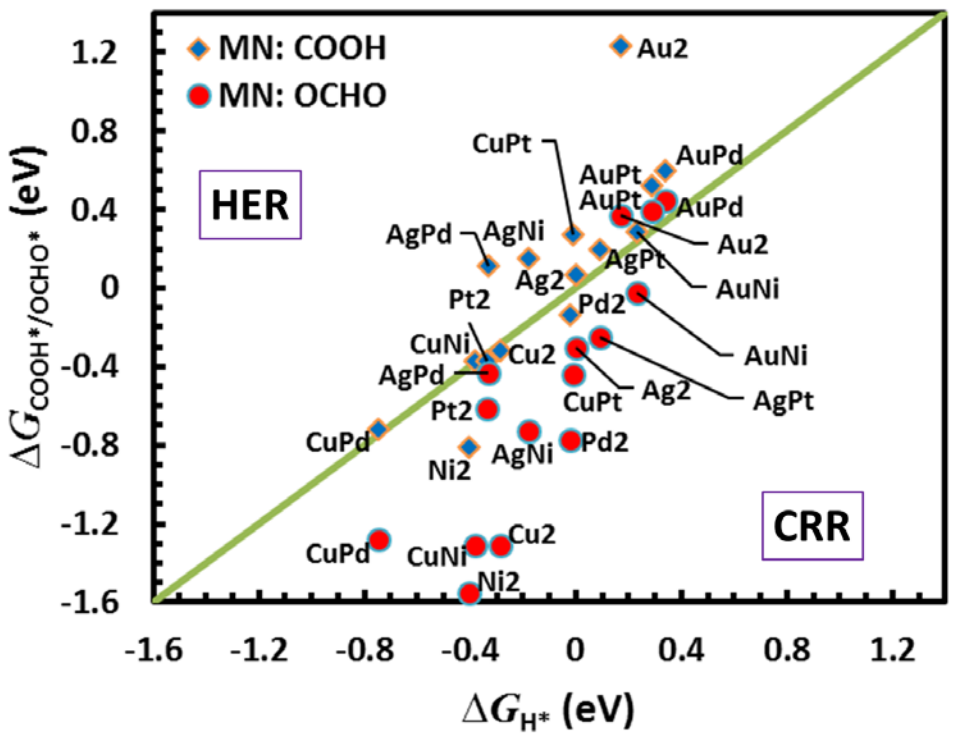

Fig. 1 First hydrogenation free energies ΔG_{COOH*} or ΔG_{OCHO*} vs. ΔG_{H*} for graphene supported homonuclear M_2 and heteronuclear MN dimers. The dimers below the bisecting line favor CRR, while the ones above favor HER.

For all OCHO* species in Figure 1 except for Au_2, AuPd and AuPt, the first hydrogenation of adsorbed CO_2 is energetically more preferable than the direct adsorption of H on the supported dimer. Since in the CHE model, the overpotential for HER by a Tafel-Vollmer mechanism is determined by the H binding energy, these results suggest the favorability of the CRR over the HER in the first step. The energetically most favorable adsorption configuration of H* is on a bridge site between two metal atoms, except for Cu_2, Pt_2, CuNi, AuPd and AuPt, where H is solely bonded to the top antenna atom; and Au_2 and AgPt, where H is solely bonded to the anchoring atom. However, no simple relationship was found between the adsorption energy of H* on monometallic dimers M_2 or bimetallic dimers MN. In summary, this step has ruled out graphene supported Au_2, AuPd and AuPt as CO_2 reduction electrocatalysts, because these dimers only

weakly bind to the hydrogenated species of CO_2– COOH* and OCHO* and more strongly bind H*, suggesting preference of HER.

3. Reaction Pathways of CO_2 Electrochemical Reduction to CH_4

The lowest energy reaction pathways for producing methane (CH_4) have been investigated for graphene supported monometallic dimers Cu_2, Ag_2, Au_2, Ni_2, Pd_2, and Pt_2, and are summarized in Figure 2 (see Supporting Information Figure S7 for structure details). Details of exploring all possible intermediates can be found in our previous publications.[12, 13] Despite the differences among these different catalysts, the reaction pathways share common traits with the graphene supported single-atom catalyzed CO_2 reduction. During this $8e^-$ reduction process, the first electron reduction favors the formation of OCHO* instead of COOH*, as discussed in Section III-2. It then follows with the second electron reduction and formation of formic acid on surface HCOOH*. With another proton and electron transfer, HCOOH* then dehydrates to produce CHO*, a critical intermediate. Note that it was verified that the energy of CHO* is lower than that of COH*. The fourth proton and electron transfer uniformly leads to the formation of CH_2O*, which is lower in energy than CHOH*. Further hydrogenation then differs for different dimers. They can be put into three categories. Cu_2, Ni_2 and Ag_2 follow the path of $CH_2O^* \rightarrow CH_3O^* \rightarrow O^* + CH_4^* \rightarrow OH^*$, which is similar to previous findings for surfaces. Pd_2 and Pt_2, instead, follows the path of $CH_2O^* \rightarrow CH_2OH^* \rightarrow CH_3OH^* \rightarrow OH^* + CH_4$. Au_2 is different from both following the path of $CH_2O^* \rightarrow CH_3O^* \rightarrow CH_3OH^* \rightarrow OH^* + CH_4$. The last step of the reaction is the same for all: the eighth proton coupled electron transfer to the surface hydroxyl group and formation of H_2O to release from the surface. By then, the $8e^-$ reduction is completed and the catalytic surface is recovered.

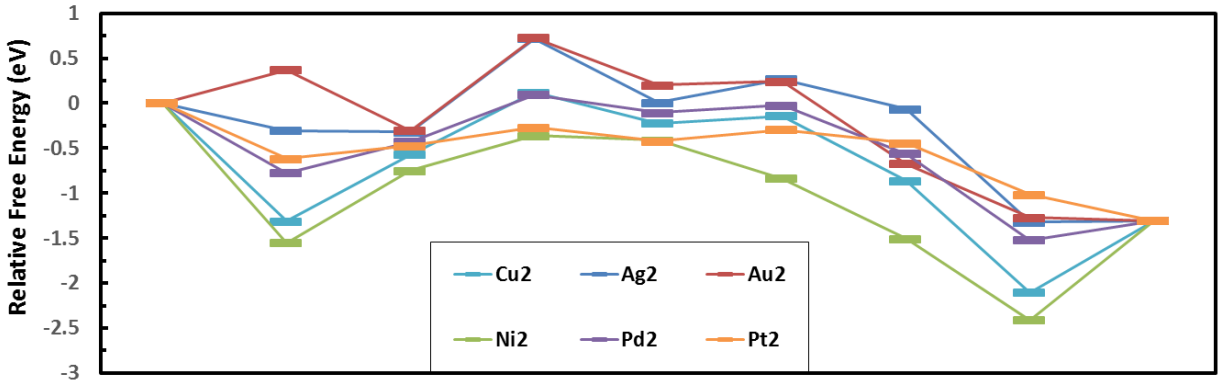

	1	2	3	4	5	6	7	8	9
Cu_2	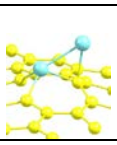	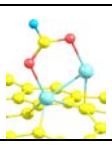			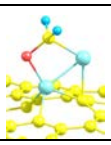		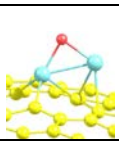	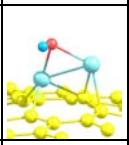	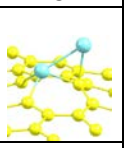
	*+CO_2	OCHO*	HCOOH*	CHO*	CH_2O*	CH_3O*	O*+CH_4	OH*	*+H_2O
Ag_2	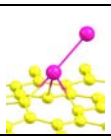	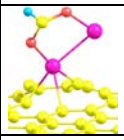		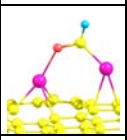	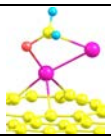		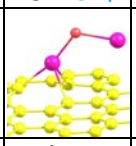	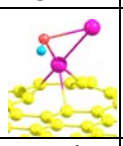	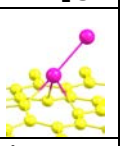
	*+CO_2	OCHO*	HCOOH*	CHO*	CH_2O*	CH_3O*	O*+CH_4	OH*	*+H_2O
Au_2		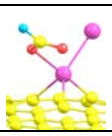		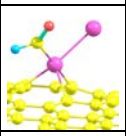	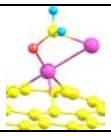	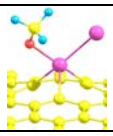			
	*+CO_2	OCHO*	HCOOH*	CHO*	CH_2O*	CH_3O*	CH_3OH*	OH*+CH_4	*+H_2O
Ni_2	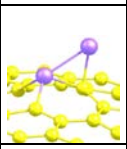		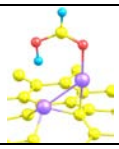		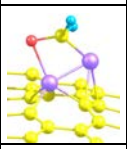	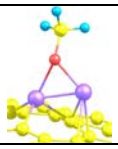	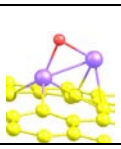	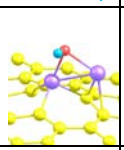	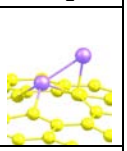
	*+CO_2	OCHO*	HCOOH*	CHO*	CH_2O*	CH_3O*	O*+CH_4	OH*	*+H_2O
Pd_2	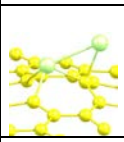		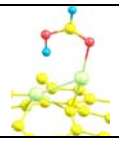						
	*+CO_2	OCHO*	HCOOH*	CHO*	CH_2O*	CH_2OH*	CH_3OH*	OH*+CH_4	*+H_2O
Pt_2									
	*+CO_2	OCHO*	HCOOH*	CHO*	CH_2O*	CH_2OH*	CH_3OH*	OH*+CH_4	*+H_2O

Fig. 2 Lowest energy reaction pathways for electrochemical reduction of CO_2 to CH_4 on a homonuclear metal dimer M_2 (M=Cu, Ag, Au, Ni, Pd, Pt) supported on graphene. Structures of surface species along the reaction pathways are denoted from 1 to 9 and shown below each of the energy steps. The energy of the initial state (denoted as 1), the gas phase CO_2 and graphene supported M_2 dimer, is taken as the reference energy of zero. Atomic symbols: Cu in light blue, Ag in pink, Au in light pink, Ni in purple, Pd in green, Pt in dark blue, C in yellow, O in red, H in blue (small).

U_L, defined as $-\Delta G/e$ (where ΔG is the elementary reaction free energy) denotes the so-called limiting potential of an elementary hydrogenation (proton coupled electron transfer) reaction when the applied electrical potential is zero. The difference between the equilibrium potential of a reduction reaction and the most negative U_L among all elementary steps along the reaction pathway represents a theoretical overpotential. By investigating the energetics of elementary hydrogenation steps as plotted in Figure 2 (also summarized in Supporting Information Table S1), it is clear that the rate limiting steps can be nailed down to three reactions (or critical elementary steps):

$$OCHO^* + H^+ + e^- \rightarrow HCOOH^* \quad (5)$$

$$HCOOH^* + H^+ + e^- \rightarrow CHO^* + H_2O \quad (6)$$

$$OH^* + H^+ + e^- \rightarrow H_2O \quad (7)$$

The first two (Reaction (5) and (6)) are involved in the generation of the intermediate CHO*; while the last one is the removal of OH*. In contrast to the single atom cases, the formation of CHO* has become the major rate limiting step for the dimers except for Cu_2 and Ni_2. The high binding strength of OH* on Cu_2 and Ni_2, makes the removal of OH* from the surface the rate limiting step for these two systems. The performance of Pt_2 and Pd_2 dimers is calculated to be the

best among the six monometallic dimers with lowest overpotentials of 0.37 V and 0.69 V, respectively, better than what was found for the single atom cases. However, both metals are highly expensive precious metals. The question would be whether it is possible to find alloy clusters with non-platinum group metal combinations that shows a reasonably low overpotential for CO_2 reduction.

4. Computational Screening of Alloy Catalytic Candidates for CH_4 Production

In the production of CH_4, the rate-limiting step could be either the release of OH* to form a H_2O molecule, the step of OCHO*→HCOOH*, or the step of HCOOH*→CHO* along the path to the formation of CHO*. Note that the binding energy of HCOOH is very similar among different dimers. By analyzing the critical steps, Cu and Ni seem to be binding to O too strongly, while Au is binding too weakly. It is a question whether an alloy combination of different metals would work constructively with their strengths and compensates for their weaknesses. We are looking for a dimer that binds to C moderately strongly (which favors Reaction (6)), while binds to O weakly (which favors Reactions (5) and (7)). However, because the binding energies of C and O tend to correlate positively with each other, there might be an optimum binding strength towards O that can be a compromise between the two binding energies according to Sabatier principle, which was previously expressed as the volcano plot.[16, 32]

We have calculated the intermediates for the three critical steps for all graphene supported bimetallic dimers composed of one metal from Group 11 and one metal from Group 10. The structures are shown in Figure 3, while the limiting potentials of elementary steps and overpotentials are summarized in Table 2. The overpotentials are calculated from the most

Table 2 Negative of the calculated elementary limiting potentials $-U_L$ (in V) required for three critical steps in the production of CH_4 for the heteronuclear dimers supported on defective graphene. The rate-limiting step is the more negative of the three. And the overpotentials (in V) are calculated from the rate limiting potential and the equilibrium potential (+0.17 V) for CO_2 electroreduction to CH_4.

	CuNi	CuPd	CuPt	AgNi	AgPd	AgPt	AuNi	AuPd	AuPt
OCHO*→HCOOH*	0.98	1.07	0.31	0.52	0.18	0.05	-0.20	-0.80	-0.65
HCOOH*→CHO*	0.11	0.33	0.61	0.39	0.86	0.59	0.83	0.87	0.71
OH*→*+H_2O	0.99	1.14	0.81	0.39	-0.13	0.15	-0.27	-0.52	-0.16
Overpotential	1.16	1.31	0.98	0.69	1.03	0.76	1.00	1.04	0.88

negative limiting potential and the equilibrium potential (+0.17 V) for CO_2 electroreduction to CH_4. The four most promising candidates, with an overpotential in increasing order of Pt_2<AgNi≈Pd_2<AgPt, have lower or competitive overpotentials to the best known single-atom catalysts Ag supported on single-vacancy graphene (0.73 V),[13] Os (0.69 V) and Ru (0.69 V) adsorbed at a divacancy graphene.[14]

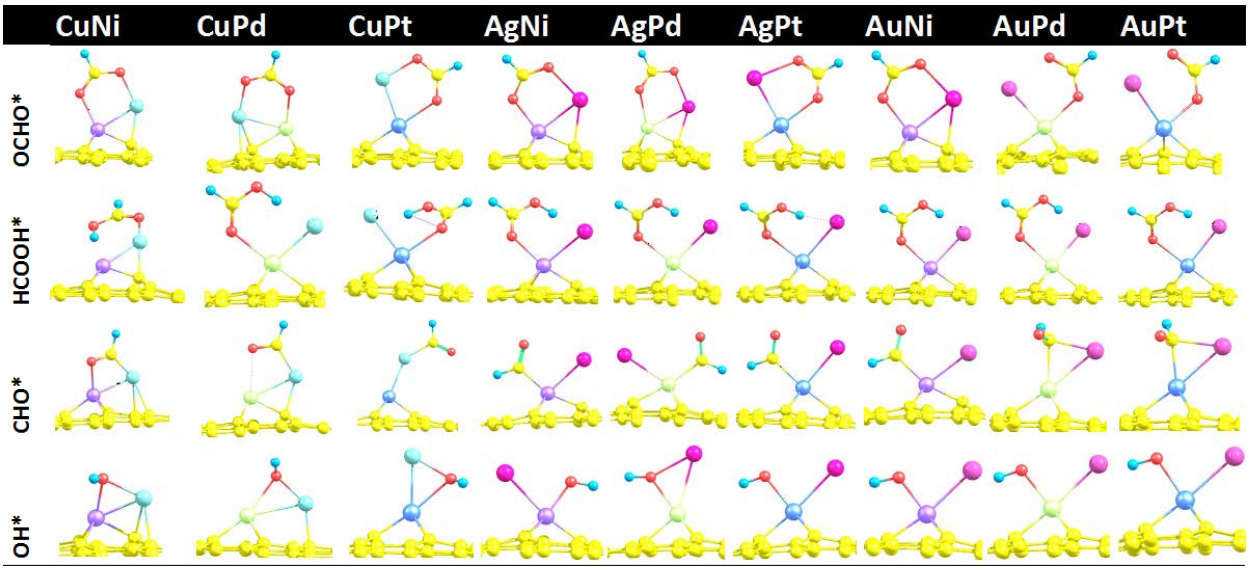

Fig. 3 Lowest energy structures of critical step intermediates of electrochemical reduction of CO_2 to CH_4 on heteronuclear bimetallic dimer MN (M=Cu, Ag, Au; N=Ni, Pd, Pt) supported on graphene. Atomic symbols are the same as in Fig. 2.

The bimetallic dimer AgNi is an attractive candidate, which has competitive performance with Pd_2, but much lower cost. It is interesting to see the synergistic effect of the alloying elements Ag and Ni. Neither of them works well by themselves. Ag_2 has a low value of $-U_L$ (0.02 V) to release the OH* group, but a significantly high value of $-U_L$ (1.04 V) to form CHO* due to the low binding strength to CHO*. Ni_2, on the other hand, requires an exceptionally high value of $-U_L$ (1.10 V) to protonate OH* and release as a H_2O molecule from the catalytic surface owing to the high binding strength to OH*. The combination of these two elements to form a dimer forces Ni to sit at the defect site of graphene and largely weakens its contribution to the adsorption of chemical species. In the meantime, it enhances the stability of the dimer on graphene as well.

In order to further investigate the connection of limiting potentials and the fundamental properties, such as the binding energy of O*, we have plotted $-U_L$ vs. E_b [O] in Figure 4. A volcano

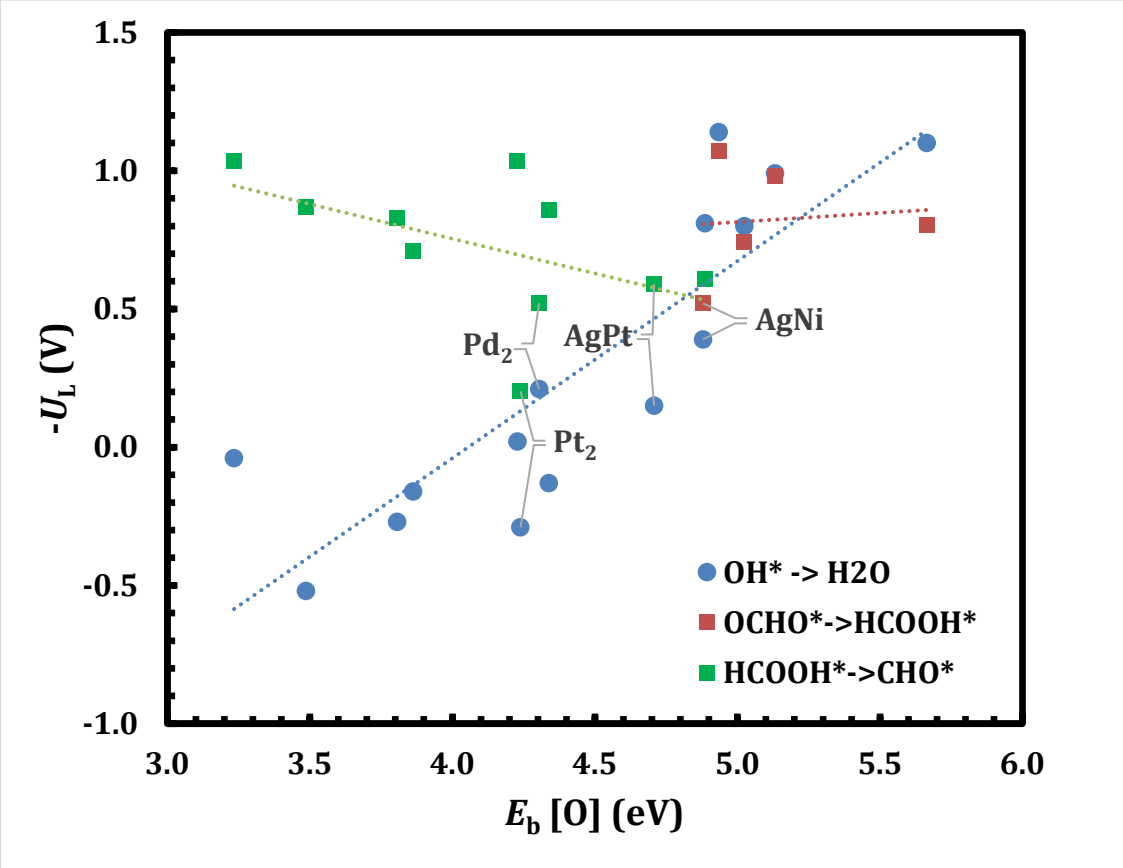

Fig. 4 Variation of the negative of rate limiting potentials (-U_L) of three critical steps with the oxygen binding energy (E_b [O]) of graphene-supported M_2 and MN catalysts for CO_2 electrochemical reduction to produce CH_4. The linear trend line is shown for each series. The four best candidates are labeled.

type nature is seen from the plot. Three critical steps (Eqn (5)-(7)) have been identified and we will discuss how they affect the overpotential in the following. The energy of OH* removal is directly related to the binding energy of O*,[26] which varies from 3.23 eV (Au_2) to 5.66 eV (Ni_2). While OH* binds weaker than O*, at higher E_b [O], the binding of OH* tends to be stronger as well resulting in a higher potential to release OH*, which is likely to be the overall rate limiting

step. This is the case for Ni_2, and Cu-containing dimers. The formation of the critical intermediate CHO* involves two elementary steps. Since OCHO* also binds through oxygens, a similar trend is observed for OCHO*→HCOOH* (Eqn (5), the first step in forming CHO*, orange squares in Figure 4), as for OH*→H_2O. On the other hand, a lower E_b [O] will lead to weaker binding of the product CHO* in the elementary step HCOOH* → CHO* (Eqn (6), green squares in Figure 4), thereby requiring a higher reaction potential. In sum, at higher E_b [O], OH*→H_2O or OCHO*→HCOOH* could be the rate limiting step, while at lower E_b [O], HCOOH*→CHO* becomes the rate limiting step. Thereby, the variation of $-U_L$ vs. E_b [O] forms a "V" shape with the lowest $-U_L$ at an optimal E_b [O] value of 4.2-4.9 eV.

What then determines the binding strength of O of an alloy dimer? Despite the overall consistency of the trend, however, there is no apparent quantitative correlation of the O binding energies on the graphene supported dimers and the single atom doped graphene. This highlights that the unique binding of dimers with the support has a significant impact on the adsorption of chemical species with these dimers. We have further explored the connection of the bimetallic dimers with the monometallic dimers. The O binding energy can be fitted into an algebraically weighted model based on the constituent elements and the preferred anchoring site on graphene fairly well (see Figure 5). The empirical relation is written below:

$$E_{b\_\mathrm{MN}}[\mathrm{O}] = 0.186E_{b\_\mathrm{N2}}[\mathrm{O}] + 0.814E_{b\_\mathrm{M2}}[\mathrm{O}] \quad (8)$$

where E_{b_MN}, E_{b_N2}, and E_{b_M2}, stand for the oxygen binding energy of the single-vacancy graphene supported bimetallic dimer MN, the monometallic dimer N_2 and M_2, respectively. Note that N is the anchoring atom, while M is the antenna atom. This fitting suggests that the antenna atom has a larger weight (~80%), i.e. a larger contribution to the overall binding to O. This is reasonable considering that O is highly electronegative and tends

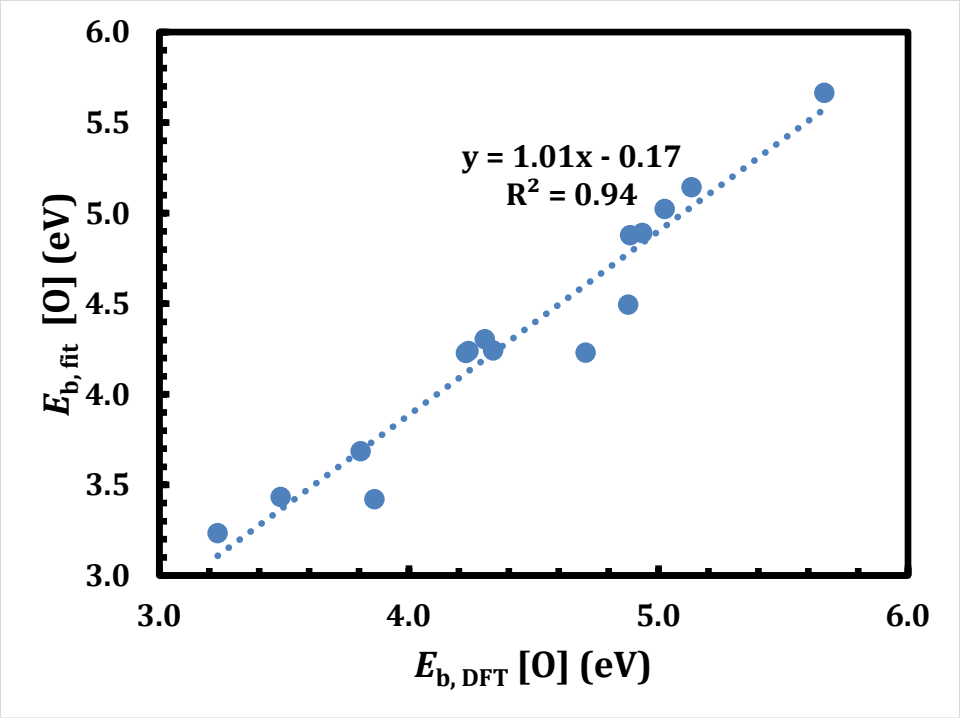

Fig. 5 Comparison of binding energy of O of dimers on single-vacancy graphene: numerical fitting based on a weighted alloy model vs. DFT calculations.

to attract electrons forming a negatively charged ion. The anchoring atom is largely positively charged and electron poor, while the antenna atom is more negatively charged.

This has an interesting implication about the right binding strength of the antenna atom. Cu_2 binds strongly to O with a binding energy of 5.02 eV, while Pd_2 binds to O with an energy of 4.30 eV appearing to be in the right binding range. In case of CuPd, we consider switching the position of Cu and Pd, i. e. Cu being the anchoring atom and Pd the antenna atom (dimer binding energy weakened by 0.64 eV). This indeed lowers the rate limiting potential for formation of CHO* from 1.08 V to 0.47 V, while negative of the limiting potential for removal of OH* decreases from 1.14 V to 0.33 V.

The breaking of the correlations among binding energies of the key intermediates OCHO*, HCOOH*, CHO* and OH* with E_b [O] indicates a good opportunity to go beyond scaling behavior and look for catalysts based on a small number of atoms that have unique properties to reduce rate limiting potentials and improve the catalytic performance.

IV. CONCLUSIONS

A dimer catalyst is the minimal bimetallic catalyst structure that can be tuned for support interactions and catalytic performance. Compared to single atom catalysts that opened up new horizons in catalysis, the dimers extend the parameter space to optimize properties. At the same time, they retain non-monotonous property relationships that provides an opportunity to break scaling relationships. Monometallic and bimetallic dimers formed from Group 10 (Ni, Pd, Pt) and group 11 (Cu, Ag, Au) elements supported at single vacancy sites of graphene are uniquely featured by an anchoring atom occupying the vacancy site with a large electron transfer to the graphene, and an antenna atom, which is much less positively charged, sticking out from the graphene surface. All the clusters can favorably bind to the defective graphene with significant binding energies suggesting their high stability. The Group 10 elements of the dimer tend to bind stronger with the graphene vacancy than the Group 11 elements. Since the stability for the alloy dimers is largely determined by the binding strength of the anchoring atoms, the stability of the alloy clusters are highly enhanced compared to the monometallic cases of Cu_2, Ag_2, and Au_2.

Potential candidates for the electrochemical reduction of CO_2 to CH_4 have been identified among these dimers through computational screening based on a first-principles approach and the computational hydrogen electrode model. We first investigated the preference of CRR vs. HER, which is true in all cases except Au_2, AuPd and AuPt. To continue, we have investigated the full

reaction pathways to generate CH_4 for monometallic dimers and identified possible rate controlling steps. In contrast to the single atom systems, where protonation of OH* to release H_2O from the metal atom is the rate limiting step, for dimers, formation of CHO* has emerged to control the overpotential to produce CH_4 in some systems. Lastly, the calculations of critical intermediates completed our screening for the potential candidates. Overall, Pt_2, AgNi, Pd_2, and AgPt are the best candidates with the lowest overpotential values of 0.37, 0.69, 0.69 and 0.76 V, respectively, which shows improved performance compared to the commonly used Cu electrodes (1.05 V) to produce hydrocarbons.[16]

While the oxygen binding strength E_b [O] of the catalytic dimer seems to provide semi-quantitative description to the reactivity of the supported dimers, the free energies of OCHO* and OH* correlate well with O*, while those of CHO* and HCOOH* have a large variation. This offers an attractive opportunity to explore breaking scaling relationships in search of better electrochemical performance.

ACKNOWLEDGMENTS

HH and CM acknowledge the funding support from the Visiting Faculty Program of the Department of Energy and the Indiana Space Grant Consortium (INSGC). Use of the Center for Nanoscale Materials, an Office of Science user facility, was supported by the U.S. Department of Energy, Office of Science, Office of Basic Energy Sciences, under Contract No. DE-AC02-06CH11357. LAC and PZ were supported by the U.S. Department of Energy, Office of Science, Office of Basic Energy Sciences, Division of Materials Science and Engineering under Contract No. DE-AC02-06CH11357

REFERENCES:

1. Kondratenko, E. V.; Mul, G.; Baltrusaitis, J.; Larrazabal, G. O.; Perez-Ramirez, J. Status and perspectives of CO2 conversion into fuels and chemicals by catalytic, photocatalytic and electrocatalytic processes. *Energy & Environmental Science* 2013, 6, 3112-3135.
2. Ampelli, C.; Genovese, C.; Marepally, B. C.; Papanikolaou, G.; Perathoner, S.; Centi, G. Electrocatalytic conversion of CO2 to produce solar fuels in electrolyte or electrolyte-less configurations of PEC cells. *Faraday Discussions* 2015, 183, 125-145.
3. Kortlever, R.; Shen, J.; Schouten, K. J. P.; Calle-Vallejo, F.; Koper, M. T. M. Catalysts and Reaction Pathways for the Electrochemical Reduction of Carbon Dioxide. *The Journal of Physical Chemistry Letters* 2015, 6, 4073-4082.
4. Lim, R. J.; Xie, M.; Sk, M. A.; Lee, J.-M.; Fisher, A.; Wang, X.; Lim, K. H. A review on the electrochemical reduction of CO2 in fuel cells, metal electrodes and molecular catalysts. *Catalysis Today* 2014, 233, 169-180.
5. Hori, Y.; Wakebe, H.; Tsukamoto, T.; Koga, O. Adsorption of CO accompanied with simultaneous charge transfer on copper single crystal electrodes related with electrochemical reduction of CO2 to hydrocarbons. *Surface Science* 1995, 335, 258-263.
6. Centi, G.; Perathoner, S.; Wine, G.; Gangeri, M. Electrocatalytic conversion of CO2 to long carbon-chain hydrocarbons. *Green Chemistry* 2007, 9, 671-678.
7. Kim, C.; Jeon, H. S.; Eom, T.; Jee, M. S.; Kim, H.; Friend, C. M.; Min, B. K.; Hwang, Y. J. Achieving Selective and Efficient Electrocatalytic Activity for CO2 Reduction Using Immobilized Silver Nanoparticles. *Journal of the American Chemical Society* 2015, 137, 13844-13850.
8. Gangeri, M.; Perathoner, S.; Caudo, S.; Centi, G.; Amadou, J.; Bégin, D.; Pham-Huu, C.; Ledoux, M. J.; Tessonnier, J. P.; Su, D. S.; Schlögl, R. Fe and Pt carbon nanotubes for the electrocatalytic conversion of carbon dioxide to oxygenates. *Catalysis Today* 2009, 143, 57-63.
9. Lim, D.-H.; Jo, J. H.; Shin, D. Y.; Wilcox, J.; Ham, H. C.; Nam, S. W. Carbon dioxide conversion into hydrocarbon fuels on defective graphene-supported Cu nanoparticles from first principles. *Nanoscale* 2014, 6, 5087-5092.
10. Vajda, S.; Pellin, M. J.; Greeley, J. P.; Marshall, C. L.; Curtiss, L. A.; Ballentine, G. A.; Elam, J. W.; Catillon-Mucherie, S.; Redfern, P. C.; Mehmood, F.; Zapol, P. Subnanometre platinum clusters as highly active and selective catalysts for the oxidative dehydrogenation of propane. *Nat Mater* 2009, 8, 213-216.
11. Tyo, E. C.; Vajda, S. Catalysis by clusters with precise numbers of atoms. *Nat Nano* 2015, 10, 577-588.
12. Liu, C.; He, H.; Zapol, P.; Curtiss, L. A. Computational studies of electrochemical CO2 reduction on subnanometer transition metal clusters. *Physical Chemistry Chemical Physics* 2014, 16, 26584-26599.
13. He, H.; Jagvaral, Y. Electrochemical reduction of CO2 on graphene supported transition metals - towards single atom catalysts. *Physical Chemistry Chemical Physics* 2017, 19, 11436-11446.
14. Back, S.; Lim, J.; Kim, N.-Y.; Kim, Y.-H.; Jung, Y. Single-atom catalysts for CO2 electroreduction with significant activity and selectivity improvements. *Chemical Science* 2017, 8, 1090-1096.
15. Hammer, B.; Norskov, J. K. Why gold is the noblest of all the metals. *Nature* 1995, 376, 238-240.
16. Peterson, A. A.; Nørskov, J. K. Activity Descriptors for CO2 Electroreduction to Methane on Transition-Metal Catalysts. *The Journal of Physical Chemistry Letters* 2012, 3, 251-258.
17. Notar Francesco, I.; Fontaine-Vive, F.; Antoniotti, S. Synergy in the Catalytic Activity of Bimetallic Nanoparticles and New Synthetic Methods for the Preparation of Fine Chemicals. *ChemCatChem* 2014, 6, 2784-2791.

18. Ma, S.; Sadakiyo, M.; Heima, M.; Luo, R.; Haasch, R. T.; Gold, J. I.; Yamauchi, M.; Kenis, P. J. A. Electroreduction of Carbon Dioxide to Hydrocarbons Using Bimetallic Cu–Pd Catalysts with Different Mixing Patterns. *Journal of the American Chemical Society* 2017, 139, 47-50.
19. Li, Y.; Su, H.; Chan, S. H.; Sun, Q. CO2 Electroreduction Performance of Transition Metal Dimers Supported on Graphene: A Theoretical Study. *ACS Catalysis* 2015, 5, 6658-6664.
20. Rêgo, C. R. C.; Tereshchuk, P.; Oliveira, L. N.; Da Silva, J. L. F. Graphene-supported small transition-metal clusters: A density functional theory investigation within van der Waals corrections. *Physical Review B* 2017, 95, 235422.
21. Kresse, G.; Furthmuller, J. Efficient iterative schemes for ab initio total-energy calculations using a plane-wave basis set. *Physical Review B* 1996, 54, 11169-11186.
22. Perdew, J. P.; Burke, K.; Ernzerhof, M. Generalized gradient approximation made simple. *Physical Review Letters* 1996, 77, 3865-3868.
23. Grimme, S. Semiempirical GGA-type density functional constructed with a long-range dispersion correction. *Journal of Computational Chemistry* 2006, 27, 1787-1799.
24. Sanville, E.; Kenny, S. D.; Smith, R.; Henkelman, G. Improved grid-based algorithm for Bader charge allocation. *Journal of Computational Chemistry* 2007, 28, 899-908.
25. Ferrante, F.; Prestianni, A.; Cortese, R.; Schimmenti, R.; Duca, D. Density Functional Theory Investigation on the Nucleation of Homo- and Heteronuclear Metal Clusters on Defective Graphene. *The Journal of Physical Chemistry C* 2016, 120, 12022-12031.
26. Nørskov, J. K.; Rossmeisl, J.; Logadottir, A.; Lindqvist, L.; Kitchin, J. R.; Bligaard, T.; Jónsson, H. Origin of the Overpotential for Oxygen Reduction at a Fuel-Cell Cathode. *The Journal of Physical Chemistry B* 2004, 108, 17886-17892.
27. Peterson, A. A.; Abild-Pedersen, F.; Studt, F.; Rossmeisl, J.; Norskov, J. K. How copper catalyzes the electroreduction of carbon dioxide into hydrocarbon fuels. *Energy & Environmental Science* 2010, 3, 1311-1315.
28. Cheng, T.; Xiao, H.; Goddard, W. A. Reaction Mechanisms for the Electrochemical Reduction of CO2 to CO and Formate on the Cu(100) Surface at 298 K from Quantum Mechanics Free Energy Calculations with Explicit Water. *Journal of the American Chemical Society* 2016, 138, 13802-13805.
29. Siegbahn, P. E. M. Trends of Metal-Carbon Bond Strengths in Transition Metal Complexes. *The Journal of Physical Chemistry* 1995, 99, 12723-12729.
30. Pauling, L. THE NATURE OF THE CHEMICAL BOND. IV. THE ENERGY OF SINGLE BONDS AND THE RELATIVE ELECTRONEGATIVITY OF ATOMS. *Journal of the American Chemical Society* 1932, 54, 3570-3582.
31. Pauling, L. *Nature of the Chemical Bond*. 3rd Ed. ed.; Cornell University Press: Ithaca, 1960.
32. Nørskov, J. K.; Abild-Pedersen, F.; Studt, F.; Bligaard, T. Density functional theory in surface chemistry and catalysis. *Proceedings of the National Academy of Sciences* 2011, 108, 937-943.

TOC graphics

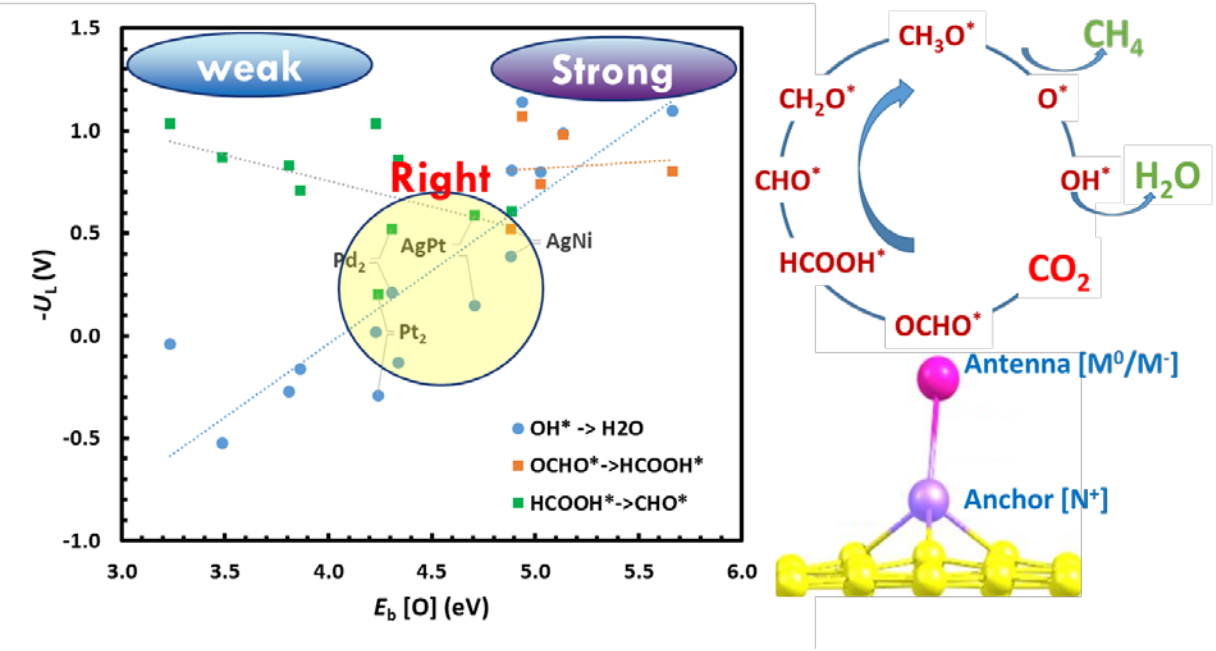

Table S1 Negative of the calculated elementary limiting potentials $-U_L$ (in V) required for three critical steps in the production of CH_4 for the homonuclear dimers supported on defective graphene. The rate-limiting step is the more negative of the three. And the overpotentials (in V) are calculated from the rate limiting potential and the equilibrium potential (+0.17 V) for CO_2 electroreduction to CH_4.

	Ni_2	Pd_2	Pt_2	Cu_2	Ag_2	Au_2
OCHO*→HCOOH*	0.80	0.35	0.14	0.74	-0.02	-0.68
HCOOH*→CHO*	0.39	0.52	0.20	0.69	1.04	1.03
OH*→*+H_2O	1.10	0.21	-0.29	0.80	0.02	-0.04
Overpotential	1.27	0.69	0.37	0.97	1.21	1.20

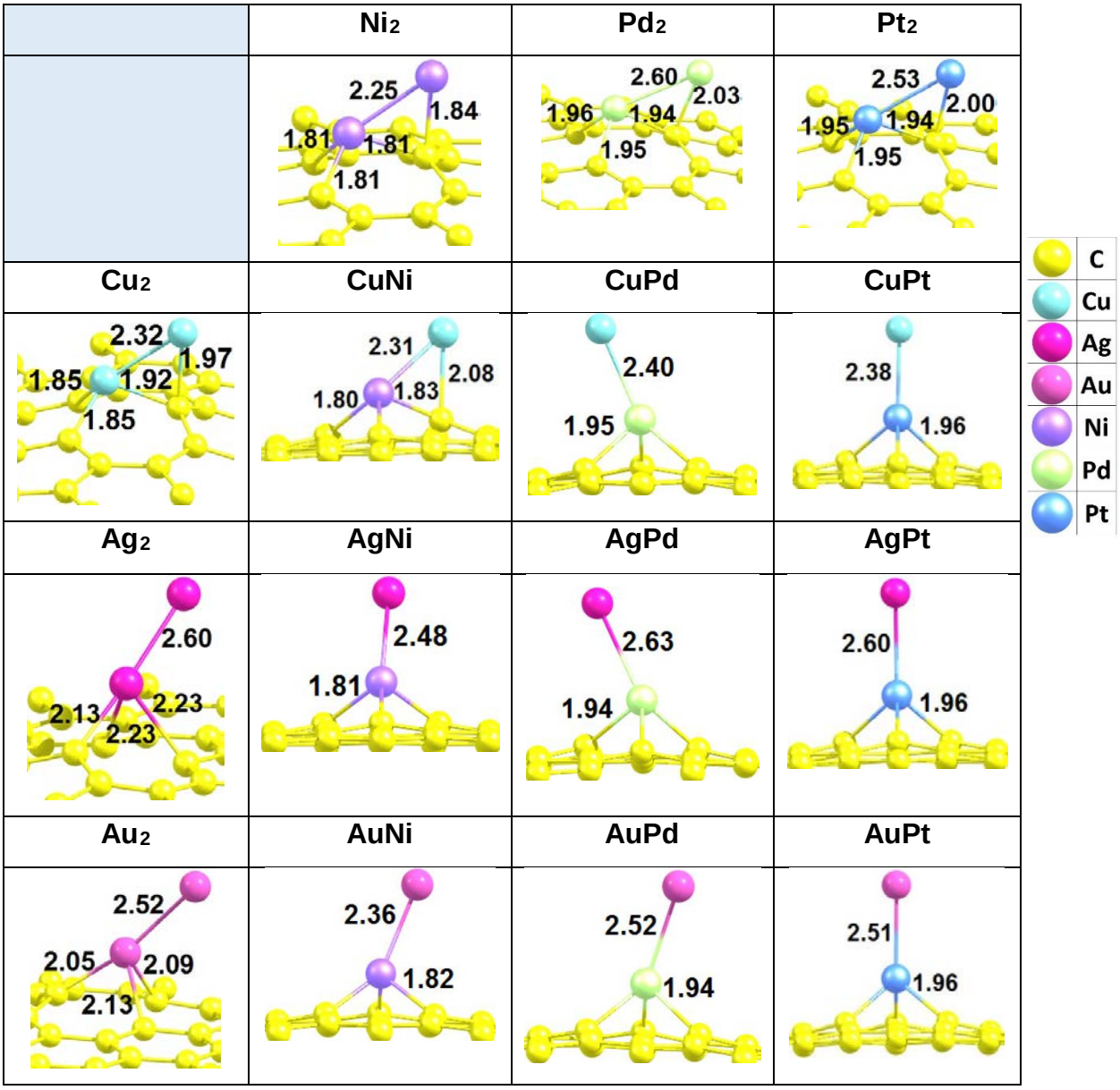

Figure S1 The most stable binding configurations of M_2/MN dimers supported on the single-vacancy site of graphene. Atomic symbols are listed on the right.

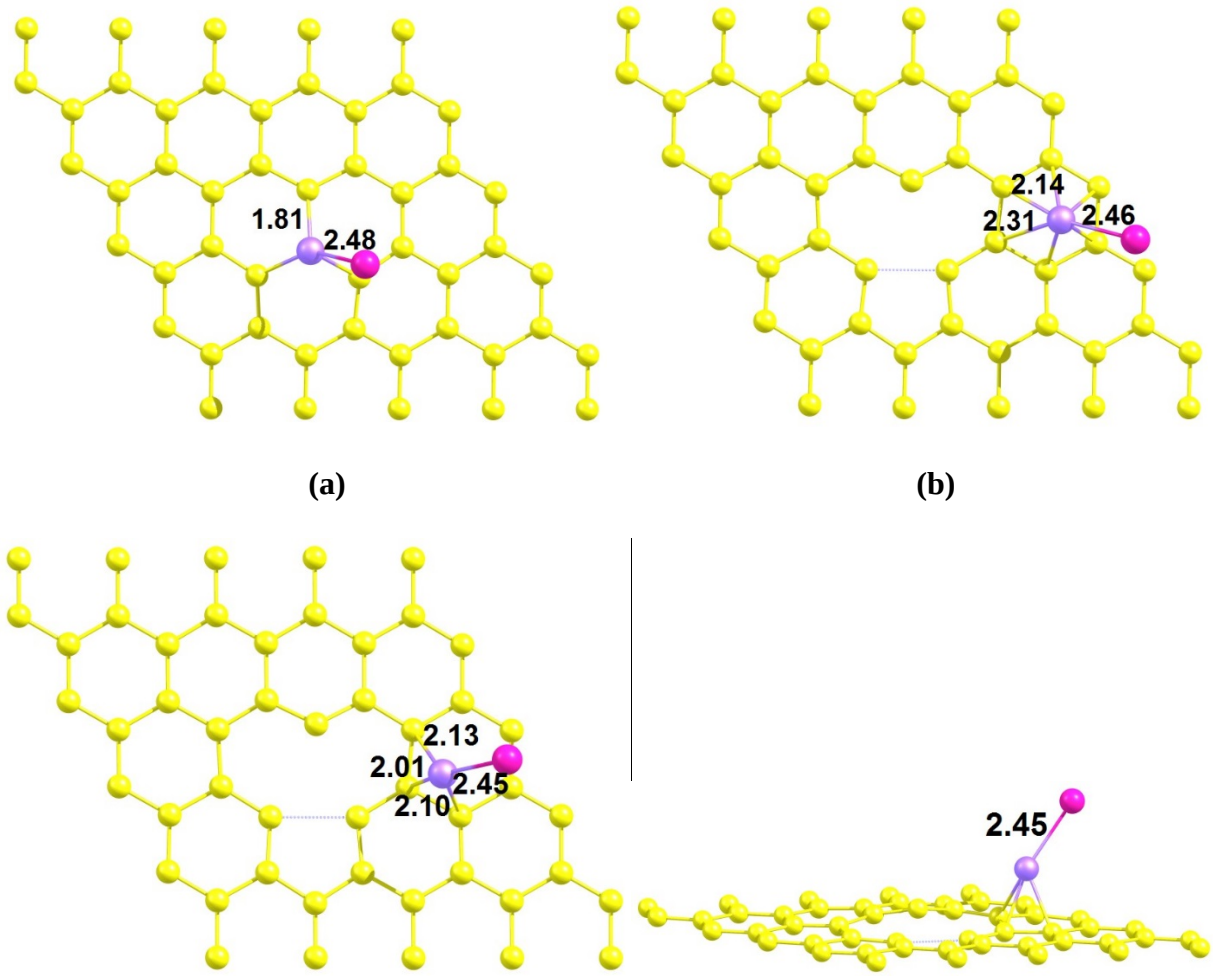

(a) **(b)**

(c)

Figure S2 The supported AgNi dimer on graphene at: (a) the most stable binding site (single C vacancy); (b) the nearest meta-stable binding site; (c) the transition state for migrating from (a) to (b) with side and top views. C: yellow, Ag: pink, Ni: purple.

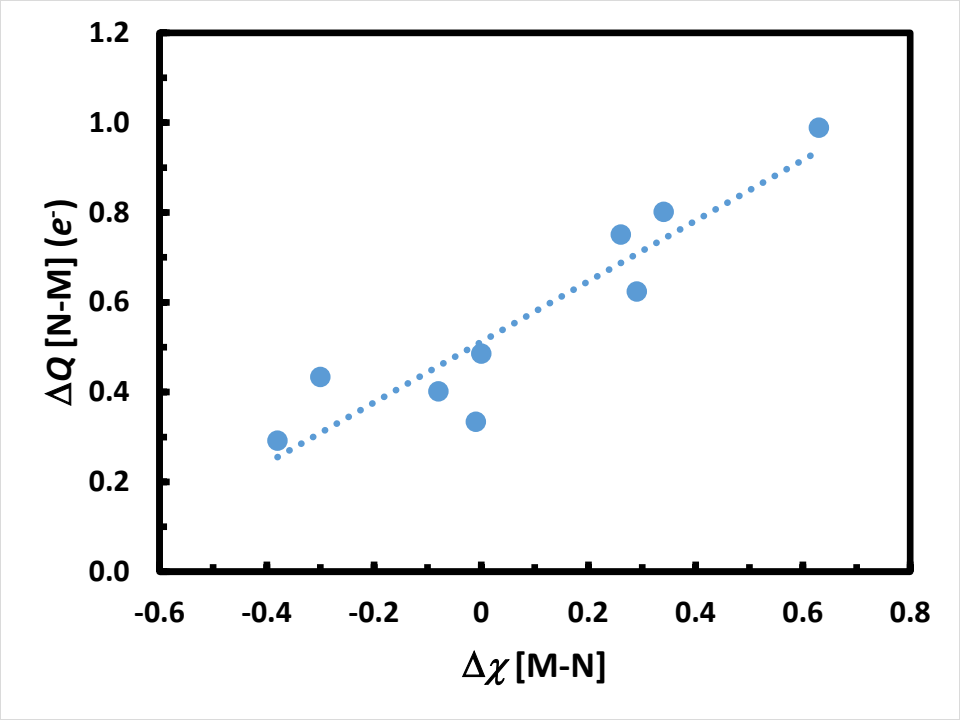

Figure S3 Correlation of the charge difference between N and M (Δ*Q* [N–M]) (M=Cu, Ag, Au; N=Ni, Pd, Pt) with the difference in their electronegativity for defective graphene supported heteronuclear metal dimers MN. The Pauling scale is adopted for the electronegativity. Note an electronegativity value of 2.2 in the Pauling scale is taken for Ag, instead of the reported value of 1.93, in observing the similarity in performance of Ag containing systems to Pd containing systems, which results in better correlation.

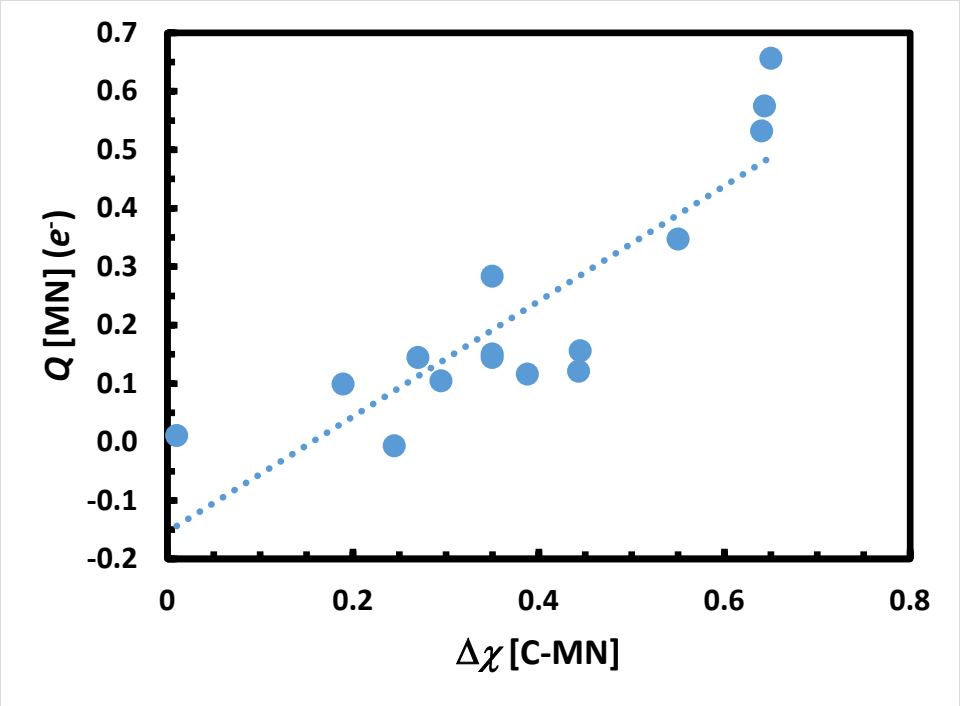

Figure S4 Correlation of the charge on the metal dimer *Q* [MN] with the difference in the electronegativity of C and the weighted value of the MN dimer for defective graphene supported metal dimers MN. The Pauling scale is adopted for the electronegativity. Note an electronegativity value of 2.2 in the Pauling scale is taken for Ag, instead of the reported value of 1.93, in observing the similarity in performance of Ag containing systems to Pd containing systems, which results in better correlation.

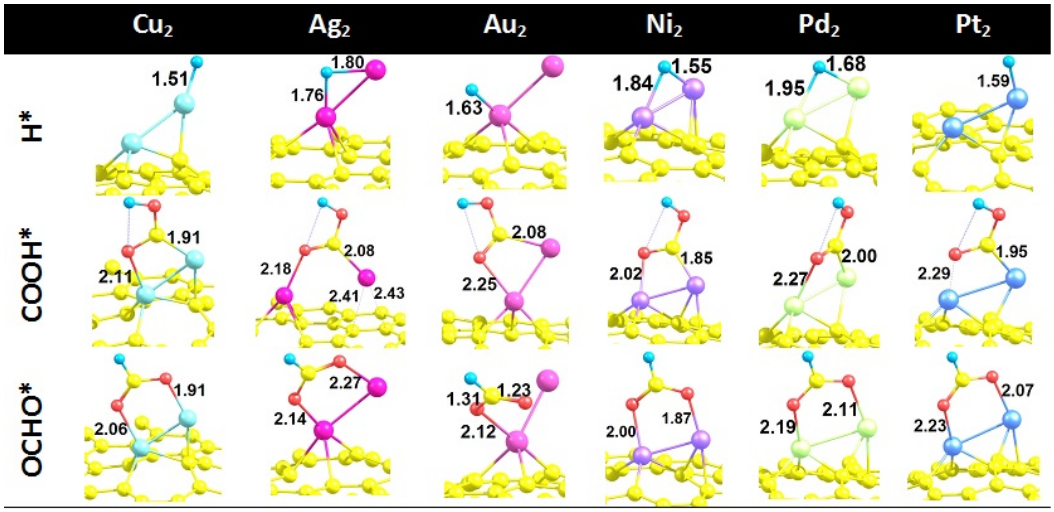

Figure S5 Lowest energy structures of the first hydrogenation species on monometallic dimers M_2 (M=Cu, Ag, Au, Ni, Pd, Pt) supported on defective graphene. Atomic symbols are the same as in Figure S1. In addition, H is in blue (small) and O in red.

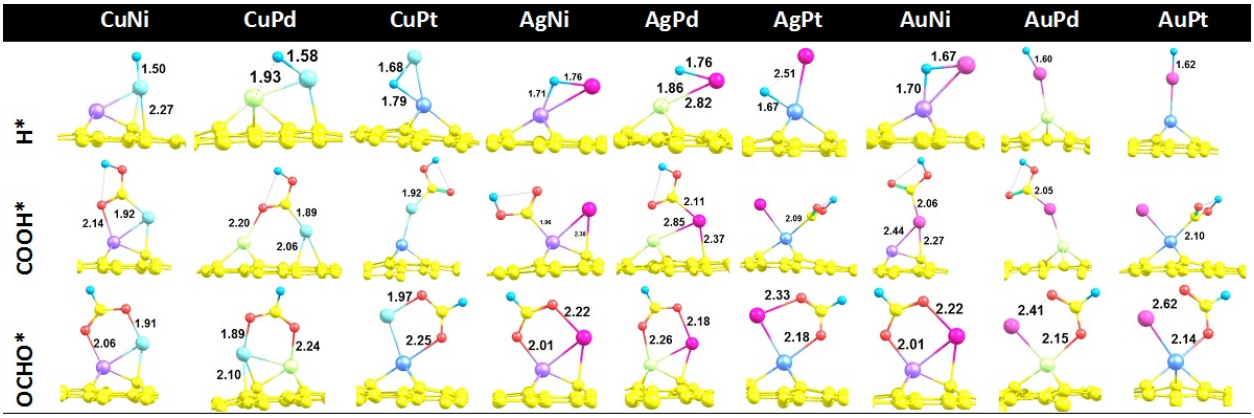

Figure S6 Lowest energy structures of the first hydrogenation species on bimetallic dimers MN (M=Cu, Ag, Au; N=Ni, Pd, Pt) supported on defective graphene. Atomic symbols are the same as in Figure S1. In addition, H is in blue (small) and O in red.

Cu_2	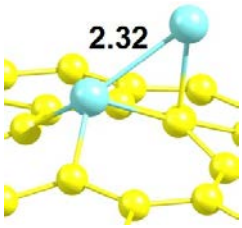	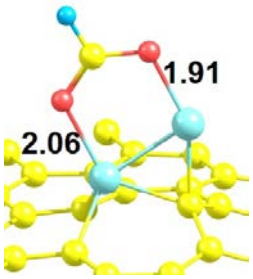	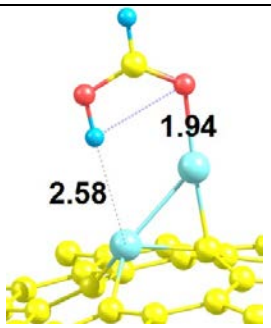
	* + C O 2	O C H O *	H C O O H *
	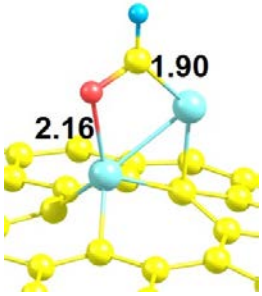	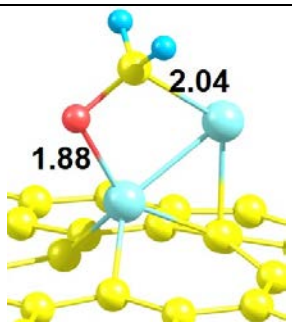	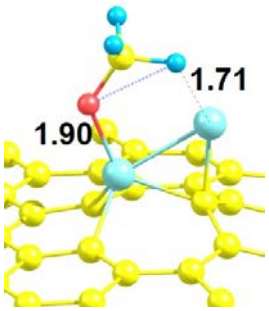
	C H O *	C H 2 O *	C H 3 O *
	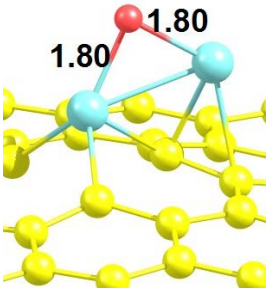	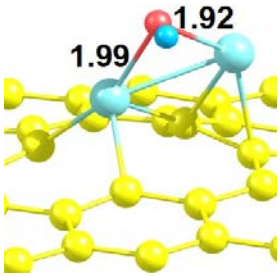	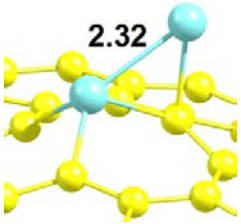
	O * + C H 4	O H *	* + H 2 O

(a)

Ag_2	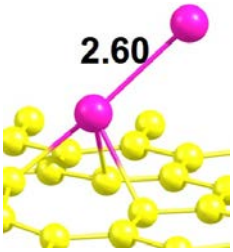	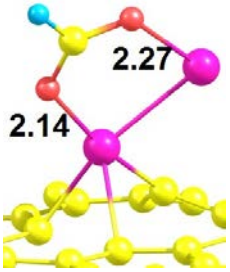	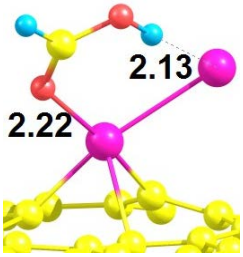
	* + C O 2	O C H O *	H C O O H *
	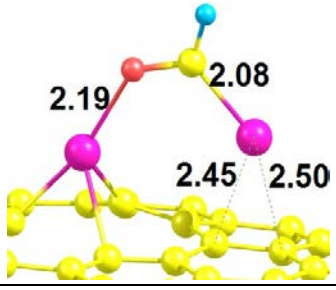	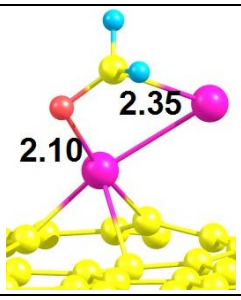	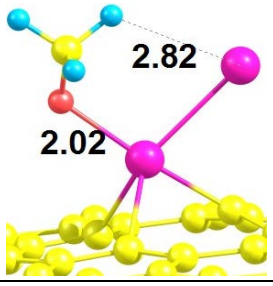
	C H O *	C H 2 O *	C H 3 O *
	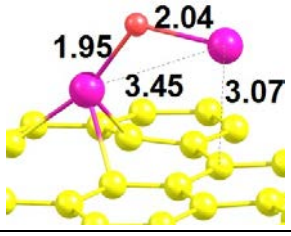	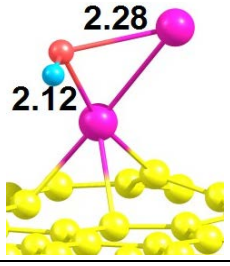	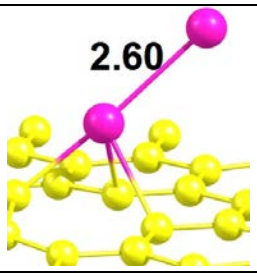
	O * + C H 4	O H *	* + H 2 O

(b)

Au_2	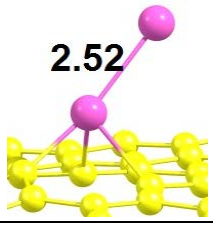	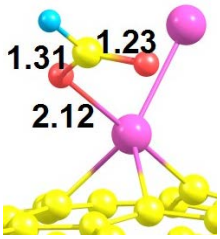	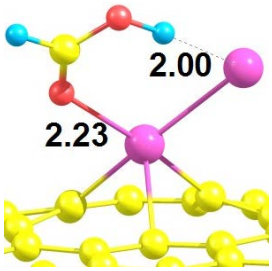
	* + C O 2	O C H O *	H C O O H *
	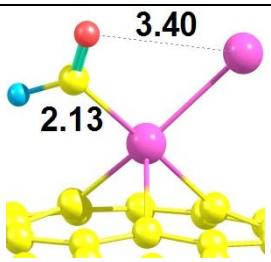	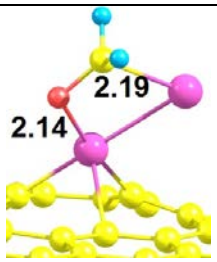	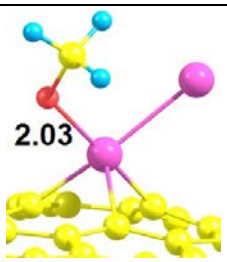
	C H O *	C H 2 O *	C H 3 O *
	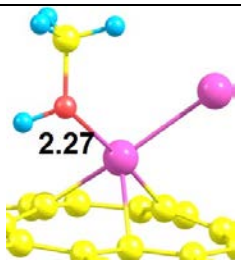	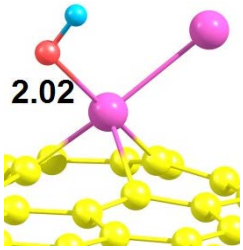	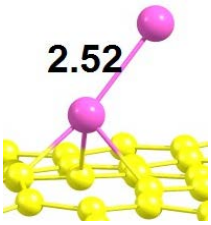
	CH 3 OH*	OH*+CH 4	* + H 2 O

(c)

Ni_2	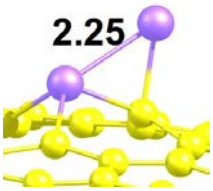	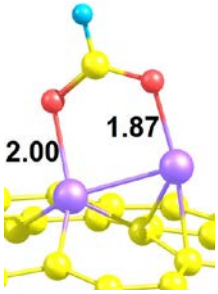	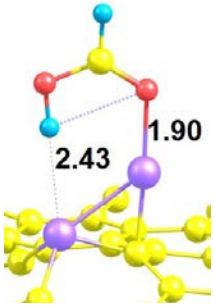
	* + C O 2	O C H O *	H C O O H *
	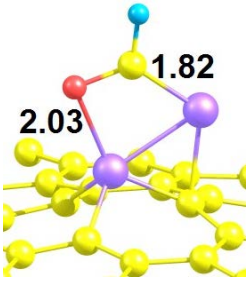	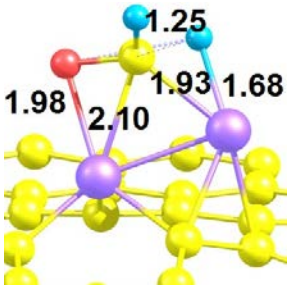	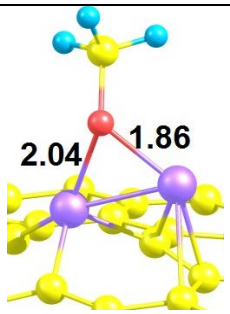
	C H O *	C H 2 O *	C H 3 O *
	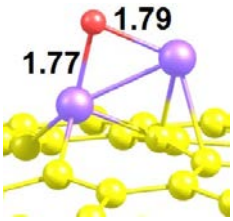	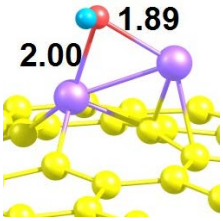	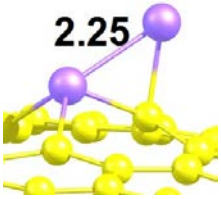
	O * + C H 4	O H *	* + H 2 O

(d)

Pd_2	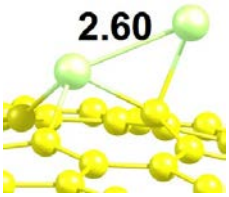	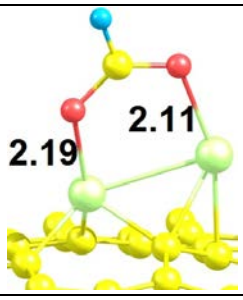	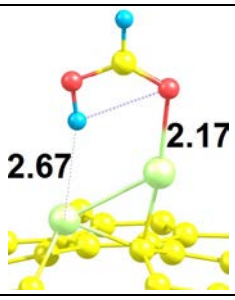
	* + C O 2	O C H O *	H C O O H *
	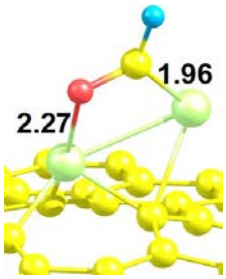	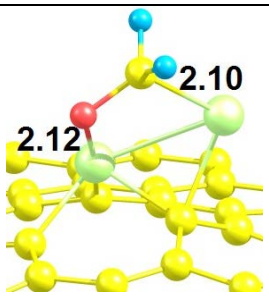	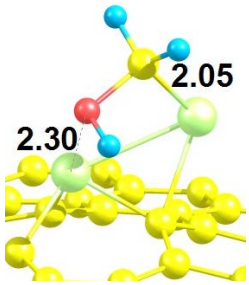
	C H O *	C H 2 O *	C H 2 O H *
	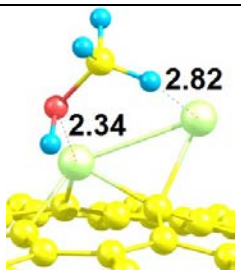	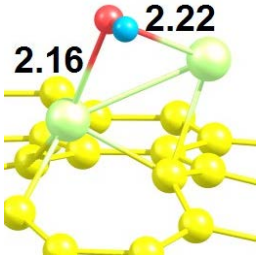	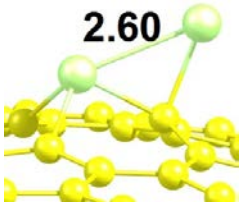
	C H 3 O H *	OH*+CH 4	* + H 2 O

(e)

Pt_2	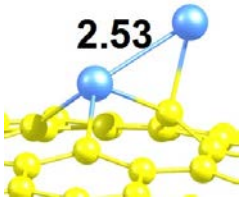	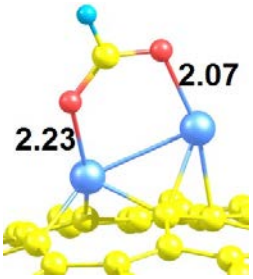	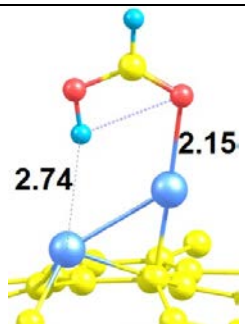
	* + C O 2	O C H O *	H C O O H *
	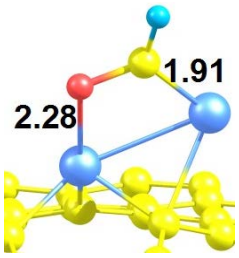	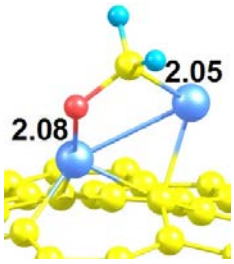	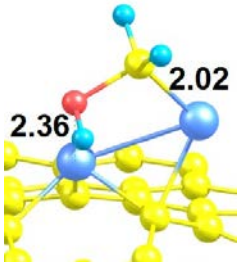
	C H O *	C H 2 O *	C H 2 O H *
	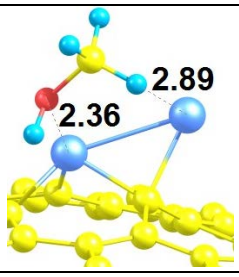	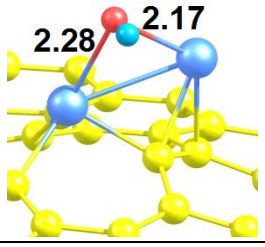	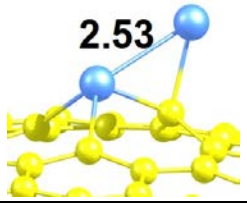
	C H 3 O H *	OH*+CH 4	* + H 2 O

(f)

Figure S7 Structures of surface species along the lowest energy reaction pathways for electrochemical reduction of CO_2 to CH_4 on a homonuclear metal dimer M_2 (M=Cu, Ag, Au, Ni, Pd, Pt) supported on graphene. Atomic symbols: Cu in light blue, Ag in pink, Au in light pink, Ni in purple, Pd in green, Pt in dark blue, C in yellow, O in red, H in blue (small).